JOURNAL OF SOLID STATE CHEMISTRY **131,** 350–357 (1997)
ARTICLE NO. SC977394

A Structural Study on the Rochelle Salt

X. Solans,* C. Gonzalez-Silgo,† and C. Ruiz-Pérez†

** Dep. Cristal.lografia, Mineralogia i Dipòsits Minerals, Universitat de Barcelona, E-08028 Barcelona, Spain and † Dep. Física Fundamental y Experimental, Universidad de la Laguna, E-38204 La Laguna, Spain*

Received September 13, 1996; in revised form March 13, 1997; accepted March 18, 1997

The crystal structure determination of Rochelle salt [$KNa(C_4H_4O_6)\cdot 4\,H_2O$] at 213, 274, and 323 K has been carried out. Crystals at 213 K are orthorhombic, $P2_12_12$, with $a = 11.880(3)$, $b = 14.298(3)$, $c = 6.216(2)$ Å, $Z = 4$, $R(F) = 0.040$. At 274 K crystals are monoclinic, $P2_1$, with $a = 11.869(3)$, $b = 14.316(8)$, $c = 6.223(3)$ Å, $\alpha = 89.26(4)^\circ$, $Z = 4$, $R(F) = 0.072$. At 323 K they are orthorhombic, $P2_12_12$, with $a = 11.924(3)$, $b = 14.298(3)$, $c = 6.230(2)$ Å. $Z = 4$, $R(F) = 0.073$. Two kinds of polarized chain in the ferroelectric phase (274 K) are observed, one similar to those found at the high-temperature paraelectric phase (323 K) and the other similar to those found at the low-temperature paraelectric phase (213 K). The paraelectric crystal structures do not show disorder or anisotropic thermal parameters which justify the hypothesis that the paraelectric–ferroelectric transition was of the order–disorder type. A study of powder diffraction, the momentum of inertia of tartrate ions, and the librational and translation tensor confirms that the transition is second order, and the independence of the two kinds of chains. A structural and thermodynamic model is proposed from these results. The ferroelectric phase is an "ordered" solid solution of two kinds of chains, which is explained from a regular model, according to which the ΔH between the two paraelectric phases is 485 cm^{-1} and w for the solid solution is 152 cm^{-1}.

INTRODUCTION

Rochelle salt is the oldest, and was for a long time the only, ferroelectric crystal known. According to early history of ferroelectricity of Busch (1), its anomalously large piezoelectric effect was notice in 1880 by the Curie brothers and quantitative measurements of its piezoelectric and electro-optic effects were carried out in 1894 by Pockels. Finally, its anomalous dielectric properties were discovered by Valasek in 1920.

The most outstanding property of Rochelle salt is that it exhibits two Curie points. The ferroelectric state is confined to the region between 291 and 249 K. The first crystal determination of the crystal structure of Rochelle salt was carried out at room temperature by Beevers and Hughes (2). Frazer *et al.* (3) attempted to determine the positions of the hydrogen atoms by neutron diffraction. Mazzi *et al.* (4), from multiple-film Weissenberg, measured only the (*hk*0) reflection at 209 and 308 K, refining the structure to *R* factors of 0.105 and 0.116, respectively. The crystal structure of the ferroelectric phase at 273 K from neutron diffraction with an electric field of 90 V cm^{-1} along the *a*-axis was isotropically refined by Mitani *et al.* (5) to an *R* of 0.102. The first anisotropic refinement was carried out by Iwata *et al.* (6) from neutron diffraction of partially deuterated Rochelle salt at 78 K. The final *R* factor was 0.073. Iwata *et al.* (7) anisotropically refined the structure of paraelectric phase at 297 K from X-ray diffraction data and Suzuki *et al.* (8) refined the ferroelectric phase at 273 K from X-ray diffraction data in a dc field of 200 V cm^{-1}.

The mechanism of ferroelectricity of Rochelle salt has been explained by the Mitsui (9) theory and its extensions (10, 11) based on the sublattice model. From the structural view, the ferroelectric phase has been explained by Pepinsky (3, 12). These authors assumed that the crystal structure of Rochelle salt is a combination of two kinds of different chains along the *a*-axis, labeled by these authors as *P* and *R*. Each chain shows a polarization, the magnitude of which is labeled also *P* and *R*, respectively. They assumed that the two paraelectric phases (the high-temperature phase for $T > 291$ K and the low-temperature phase for $T < 249$ K) are a solid solution of chains *P* and *R*, each asymmetric unit being a mixture of the two chains (they assumed the paralectric phases as disordered structures) showing a polarization $R' = 1/2[P + R]$, while the total polarization is equal to 0 by the crystal symmetry. The ferroelectric phase shows a regulating distribution of chain *P* and *R*, giving a total polarization $P + R$. However, for confirmations of details, precise information about the ferroelectric and paraelectric structures is required, which is the purpose of this study.

EXPERIMENTAL

Crystal growth. Crystals were grown by slow cooling between 293.3 and 296.3 K at 0.3 K/day. The apparatus included a 1-liter sealed glass cylinder with two openings, one for the seed-supporting rod. Four well-shaped seeds

0022-4596/97 $25.00

of 1 cubic millimeter size of Rochelle salt were selected by optical microscope examination, glued with silicon, and suspended in the aqueous solution. The seeds underwent alternate accelerated and decelerated rotation, varying the angular velocity from 0 to 5 rpm. A rest period of 2 s was left to allow the entire solution to become completely still. No disturbances due to acceleration and deceleration vibrations were observed. The temperature control of the apparatus was by immersion of the sealed glass cylinder in a 5-liter oil-filled thermostat equipped with a stirrer. The oil bath temperature was controlled by a Eurotherm 818P electronic regulator with a *J*-type thermocouple with a sensitivity of 0.01 K and a regulator thyristor of 240V/15A.

X-ray powder diffraction. Powder diffraction data were collected with a Siemens D500 automated diffractometer at different temperatures, using Cu$K\alpha$ radiation and a secondary monochromator. Two similar experiments were carried out using different samples. A warming process from 298 K to T_{max} was followed by a cooling process from T_{max} to T_{min}, a further warming process from T_{min} to T_{max}, and a cooling process from T_{max} to 298 K. The T_{min} and T_{max} values for every process were 228 and 318 K and 233 and 333 K, respectively. The cooling and warming rates were 10 K/min, and the sample was left for 10 min at measuring temperature to stabilize the equipment and the sample. Measurements were taken every 10 K in the first experiment. In the second experiment the X-ray patterns were measured at 298, 308, 318, and 333 K, during the first warming; otherwise, this process was the same as the first. The step size was 0.025°, the time of the step was 10 s, and the 2θ range was 16°–120°. Cell parameters (Fig. 1) from powder diffraction were refined with the CELREF computer program (13).

X-ray structure determination. A similar method was followed in all crystal structure determinations, using a different crystal. Diffraction data were collected on an Enraf–Nonius CAD4 automated diffractometer equipped with a graphite monochromator. The ω-θ scan technique was used to record the intensities. Scan widths were calculated as $A + B\tan\theta$, where A is estimated from the mosaicity of the crystal and B allows for the increase in peak width due to Mo$K\alpha_1$–$K\alpha_2$ splitting.

Details of the structure determination are listed in Table 1. The unit cell parameters were obtained by a least-

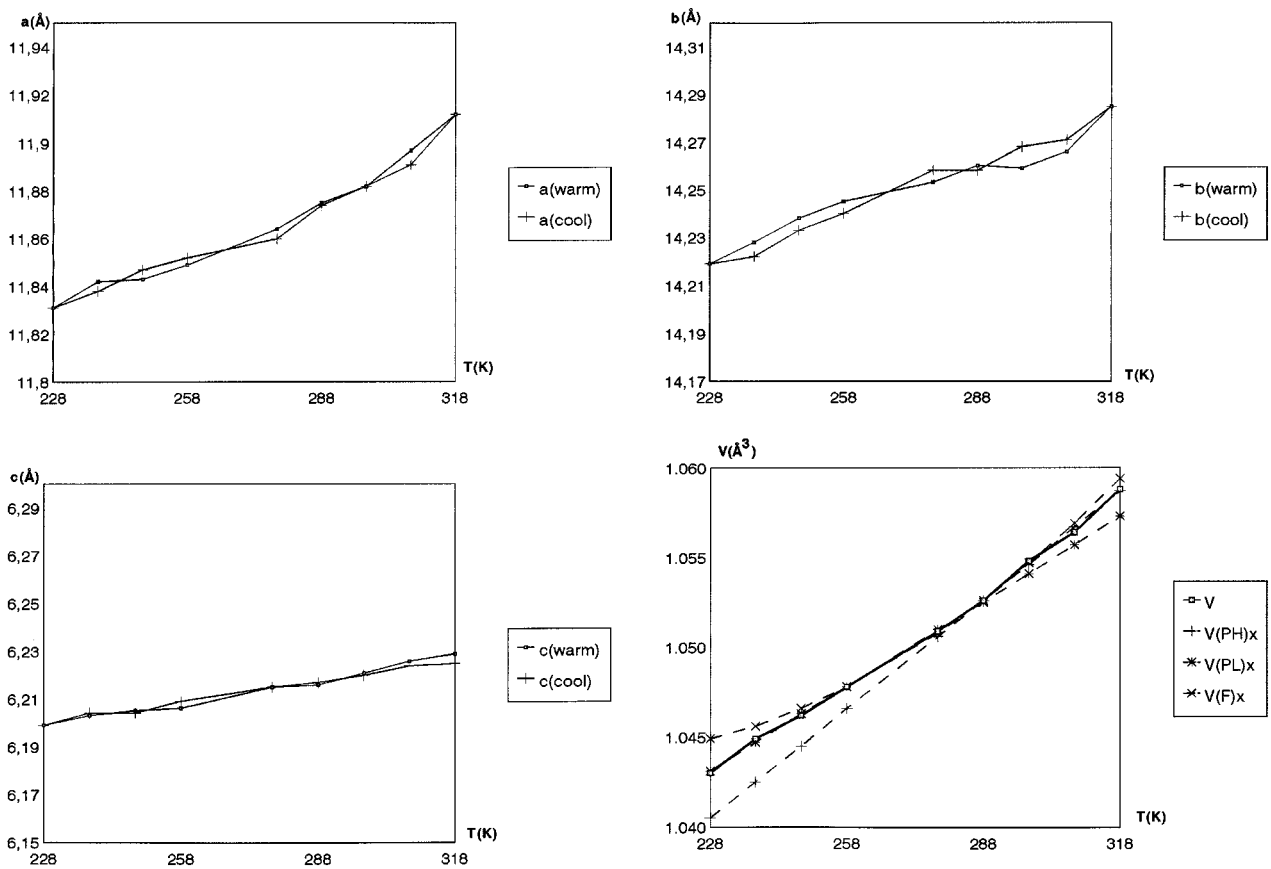

FIG. 1. Cell parameters and volume cell versus temperature, obtained from X-ray diffraction on powder samples.

TABLE 1
Crystal Data and Structure Refinement

	213 K	274 K	323 K
Empirical formula	$C_4H_{12}KNaO_{10}$		
Formula weight	282.23		
Wavelength (Å)	0.71069		
Crystal system	orthorhombic	monoclinic	orthorhombic
Space group	$P2_12_12$	$P2_1$	$P2_12_12$
a (Å)	11.880(3)	11.869(3)	11.924(3)
b (Å)	14.298(3)	14.316(8)	14.298(3)
c (Å)	6.216(2)	6.223(3)	6.230(2)
α (°)	90.00	89.26(4)	90.00
Volume(Å^3)	1055.9(5)	1057.3(8)	1062.1(5)
Z	4	4	4
ρ_x (Mg/m^3)	1.775	1.773	1.765
μ (mm^{-1})	0.585	0.584	0.582
F (000)	584	584	584
Crystal size (mm)	$0.2\times0.2\times0.3$	$0.1\times0.2\times0.3$	$0.2\times0.2\times0.3$
T range (°)	2.23–30.06	1.42–30.16	2.22–29.98
Index ranges	$-16\le h\le 16$	$-16\le h\le 16$	$0\le h\le 16$
	$-19\le k\le 20$	$0\le k\le 20$	$0\le k\le 20$
	$0\le l\le 8$	$-8\le l\le 8$	$0\le l\le 8$
Reflections collected	6120	6120	3078
Independent reflections	3078	4151	3078
R(int)	0.032	0.046	0.00
Data/parameters	3028/184	4101/335	1402/171
S on F^2	0.889	1.011	1.074
R on $F[I>2\sigma(I)]$	0.040	0.072	0.0730
wR on I	0.096	0.196	0.2032
Absolute struct.	0.03(4)	0.00(7)	−0.09(13)
Extinction coef.	0.107(7)	0.006(6)	0.001(9)
Largest diff. peak (e Å^{-3})	0.42	0.82	0.85
Largest diff. hole (e Å^{-3})	−0.62	−0.95	−0.71

squares fit to the automatically centered settings from 25 reflections ($12^\circ < 2\theta < 21^\circ$). The intensities from three control reflections for each measurement showed no significant fluctuation during the data collection at 213 or 323 K, while this fluctuation was important at 274 K.

There are two problems in the crystal structure determination of Rochelle salt at 274 K: The first is the instability of crystals according to humidity, which has not been mentioned by previous authors but was discussed by Mason (14). The second is the possible formation of ferroelectric domains, which has been largely studied by Mikaya (15), and Chernysheva *et al.* (16). The method used by Mitani *et al.* (5) and Suzuki *et al.* (8) for the crystal structure determination was to prepare a cylindrical crystal with the cylindrical axis aligned along the *a*-axis (ferroelectric axis) and attach an electrode at the both ends of crystal to obtain a monodomain crystal. This method gives rise to new problems: (a) The great size of crystal which increases the absorption effect and the number of defects, (b) the increase in dark zones for detector, and (c) the difficulty of obtaining an accurate orientation matrix. They can be observed from the high R factor obtained by the previous authors. We think that Rochelle salt does not have a high polarization value (17), so the possible ferroelectric domains are not very important, and using a smaller crystal we reduce the three mentioned problems.

To improve the crystal structure determination at 274 K, every reflection was measured to four different orientations. The reflections with asymmetric background (the left background is not similar to the right background) were not assumed. The reflections were merged (1841 reflections of the 6120 measured were not used in the merging process, according to the previous criterion). Intensity data for all structures were corrected for Lorentz and polarization effects, as well as anomalous dispersion effects, and at 274 K intensities were corrected for the decay of intensity effect. Absorption corrections were not applied.

The structures were solved by Patterson synthesis, using the SHELXS-86 computer program (18) and refined by the full-matrix least-squares method, using the SHELX-93 computer program (19). The function minimized was $w||F_o|^2 - |F_c|^2|^2$, where the weighting scheme was $w = [\sigma^2(I) + (k_1P)^2 + k_2P]^{-1}$ and $P = (|F_o|^2 + 2|F_c|^2)/3$. The values of k_1 and k_2 were, respectively, 0.0631 and 0.5551 at 213 K, 0.1539 and 1.2396 at 274 K, and 0.1706 and 0.5501 at 323 K. The chirality of the structure was defined from the Flack coefficient (20).

Study on moments of inertia and translational and librational tensors at different temperature. We have used the EKRT computer program (21), where the thermal coefficients of tartrate ion are set equal to $GL + HS + T$, T; L and S are the translational and librational tensors and G and H are the geometrical matrices which connect the atomic positions and the mass center. The function minimized was $\sum\sigma^{-1}(U_c - U_o)^2$, where U_c and U_o are the computed and observed thermal parameters matrices. Results are given in Table 2. Where it is observed, the moment of inertia is practically constant, which justifies the assumption of tartrate ions as a rigid body. The translation principal values are higher in the phase at high temperature, which agrees with the thermal vibration.

RESULTS AND DISCUSSION

X-Ray Powder Diffraction

Cell parameters were refined using all identified maxima (from 50 to 59 reflections). The monoclinic splitting for the ferroelectric phase was clearly observed in only three peaks, so the α angle was not refined. The values obtained in the first cycling experiment are shown in Fig. 1, and they are systematically 0.010 Å lower than those found by Bronowska (22) from four reflections, using the Bond method on a single crystal. This systematic difference is also observed if the values of Bronowska are compared with those of the literature obtained by single-crystal diffractometry from 25 reflections (2–4, 7). A comparison between the cell parameters obtained during the cooling and

TABLE 2
Moments of Inertia and Principal Values of the Translational and Vibrational Tensor of Tartrate Ion with the Direction Cosines, the First Referenced to Crystal Cartesian Axes, and the Second and Third Referenced to Inertial Axes

	213 K	274 K		323 K
		Ion A	Ion B	
		Principle moments of inertia		
Axis 1	589.67	591.95	580.66	584.52
Axis 2	575.61	579.33	566.77	572.97
Axis 3	185.94	183.01	185.12	182.94
Direction cosines				
Axis 1	0.83 −0.43 0.37	0.84 −0.41 0.36	0.86 −0.40 −0.33	0.85 −0.40 0.34
Axis 2	0.56 0.66 −0.50	0.55 0.66 −0.51	0.52 0.68 0.52	0.52 0.68 −0.52
Axis 3	−0.03 0.62 0.79	−0.02 0.62 0.78	0.02 −0.61 0.79	−0.02 0.62 0.78
		Principal values of translational tensor		
	0.011	0.011	0.016	0.029
	0.017	0.017	0.051	0.014
	0.015	0.051	0.013	0.022
Direction cosines				
Value 1	0.70 −0.50 −0.51	0.97 −0.23 0.13	0.86 0.52 −0.02	0.72 0.69 −0.04
Value 2	0.56 0.83 −0.04	0.25 0.94 −0.23	−0.52 0.86 −0.04	−0.53 0.58 0.62
Value 3	0.45 −0.25 0.86	−0.07 0.26 0.96	−0.00 0.04 1.00	0.45 −0.42 0.79
		Librational tensor		
	3.8	4.4	4.4	4.5
	6.2	9.7	8.6	10.6
	10.7	14.2	14.0	19.0
Direction cosines				
Value 1	0.91 0.25 −0.320	0.93 0.30 −0.19	0.64 0.77 0.07	0.89 0.41 −0.20
Value 2	−0.19 0.96 0.20	−0.25 0.93 0.28	0.74 −0.64 0.23	−0.43 0.90 −0.05
Value 3	0.36 −0.12 0.93	0.26 −0.21 0.94	−0.22 0.10 0.97	0.16 0.13 0.98

warming processes does not show a thermal hysteresis in the Rochelle salt so the two ferroelectric–paraelectric transitions are second-order transitions. The cell volume of paraelectric phases follows the equations $1007.28 + 0.157\ T$ and $994.44 + 0.202\ T$ for the low- and high-temperature phases, respectively. The cell volume for the ferroelectric phase follows the equation $1086.82 - 0.432\ T + 0.00109\ T^2$.

The second cycling process shows the decomposition of Rochelle salt to $K_2[C_4H_4O_6]\cdot 1/2\ H_2O$ and $Na_2[C_4H_4O_6]\cdot 2H_2O$ at 333 K. After cooling the sample to 233 K (260 min), the Rochelle salt is again obtained. Cell parameters obtained during the second warming process do not differ from those obtained in the first cycling process. So, the decomposition process of Rochelle salt, which was assumed as irreversible by Cady (23), is in fact reversible after a cooling process.

X-Ray Crystal Structure

Description of structures. Atomic coordinates and equivalent isotropic temperature coefficients are listed in Table 3. Selected bond length and angles are listed in Table 4. A projection down the *c*-axis of the structure at 213 K with the label of atoms is shown in Fig. 2. The Rochelle salt is composed of a row of tartrate ions parallel to the [100] axis, linked along the [010] axis by rows of alternating K and Na ions. These (001) layers are linked along the [001] direction by the K(2) ion, so every tartrate ion is surrounded by six tartrates ions. K(1) and Na(1) act as a bridge between two tartrate ions, while K(2) acts as a bridge between four tartrate ions.

The K ions display a bicapped trigonal prism coordination. The K(1) is linked with the shortest length to two oxygen atoms of different acetato groups and to six oxygen atoms of water molecules. The K(2) ion is linked to two oxygen atoms of acetato groups, two oxygens of OH groups, and four oxygens of water molecules. The shortest K(2)–O bond length is K(2)–O(7), where O(7) is an oxygen of a water molecule. The Na ions display a distorted octahedral coordination, being linked to two O (acetato), one O (OH), and three O (water). The longer and more asymmetric hole occupied by the K ions is the K(1) site. The

TABLE 3
Atomic Coordinates ($\times 10^4$) and Equivalent Isotropic Displacement Parameters ($Å^2 \times 10^3$)

	x	*y*	*z*	*U*(eq)
		213 K		
K(1)	0	0	441(1)	39(1)
K(2)	0	5000	1600(1)	24(1)
Na(1)	2322(1)	−68(1)	5185(1)	19(1)
O(1)	1201(1)	1088(1)	3488(2)	19(1)
O(2)	2115(1)	2036(1)	1178(2)	22(1)
O(3)	2305(1)	4068(1)	8171(2)	28(1)
O(4)	502(1)	3602(1)	8463(2)	26(1)
O(5)	1646(1)	3578(1)	3241(2)	19(1)
O(6)	2961(1)	2487(1)	6313(2)	21(1)
O(7)	3961(1)	833(1)	4846(2)	25(1)
O(8)	2399(2)	414(1)	8821(2)	36(1)
O(9)	4402(1)	3059(2)	10331(3)	37(1)
O(10)	4227(1)	3941(1)	4275(3)	35(1)
C(1)	1549(1)	1880(1)	2837(2)	15(1)
C(2)	1250(1)	2736(1)	4230(2)	14(1)
C(3)	1779(1)	2636(1)	6467(2)	16(1)
C(4)	1503(2)	3508(1)	7828(2)	19(1)
		274 K		
K(1)	−5(2)	2500(1)	448(3)	63(1)
K(2)	3(1)	7500(1)	1595(2)	38(1)
Na(1A)	2316(1)	2434(2)	5219(3)	31(1)
O(1A)	1199(2)	3600(3)	3523(6)	29(1)
O(2A)	2104(3)	4536(3)	1183(6)	34(1)
O(3A)	2325(4)	6564(3)	8155(8)	45(1)
O(4A)	532(3)	6124(4)	8454(8)	47(1)
O(5A)	1642(3)	6081(3)	3235(6)	32(1)
O(6A)	2958(2)	4984(3)	6282(7)	37(1)
O(7A)	3955(3)	3317(3)	4825(7)	39(1)
O(8A)	2439(5)	2925(4)	8878(8)	55(1)
O(9A)	4388(3)	5522(4)	10346(8)	55(1)
O(10A)	4231(3)	6425(4)	4242(11)	59(2)
C(1A)	1555(3)	4386(4)	2850(7)	28(1)
C(2A)	1247(3)	5227(4)	4213(8)	28(1)
C(3A)	1784(3)	5148(4)	6474(8)	30(1)
C(4A)	1518(4)	6013(4)	7808(8)	35(1)
Na(1B)	−2315(1)	2570(2)	5213(4)	33(1)
O(1B)	−1193(2)	1413(3)	3501(6)	32(1)
O(2B)	−2106(3)	472(3)	1183(6)	38(1)
O(3B)	−2329(4)	−1564(3)	8125(7)	43(1)
O(4B)	−528(3)	−1113(3)	8438(6)	41(1)
O(5B)	−1630(3)	−1066(3)	3245(6)	32(1)
O(6B)	−2953(3)	17(3)	6283(7)	36(1)
O(7B)	−3957(3)	1673(3)	4841(7)	37(1)
O(8B)	−2416(5)	2088(4)	8838(8)	57(1)
O(9B)	−4384(4)	−520(5)	10358(9)	62(2)
O(10B)	−4245(3)	−1471(4)	4210(10)	60(2)
C(1B)	−1540(3)	624(4)	2859(7)	27(1)
C(2B)	−1249(3)	−238(4)	4228(8)	29(1)
C(3B)	−1778(3)	−141(4)	6452(7)	27(1)
C(4B)	−1520(4)	−1002(4)	7821(7)	30(1)
		323 K		
K(1)	0	0	470(3)	63(1)
K(2)	0	5000	1586(2)	34(1)
Na	2312(2)	9932(1)	5234(3)	28(1)
O(1)	1205(3)	1094(2)	3500(6)	29(1)
O(2)	2102(4)	2028(2)	1189(5)	35(1)
O(3)	2322(4)	4062(2)	8119(6)	39(1)
O(4)	540(4)	3629(3)	8428(6)	39(1)
O(5)	1636(3)	3567(2)	3221(5)	27(1)
O(6)	2954(3)	2484(2)	6274(6)	30(1)
O(7)	3964(3)	825(2)	4842(7)	37(1)
O(8)	2429(6)	413(2)	8872(6)	51(1)
O(9)	4378(5)	3004(5)	366(9)	62(1)
O(10)	4242(4)	3967(4)	4227(11)	57(1)
C(1)	1545(3)	1879(2)	2849(6)	20(1)
C(2)	1249(3)	2732(2)	4235(6)	32(1)
C(3)	1791(3)	2644(2)	6451(6)	21(1)
C(4)	1537(5)	3516(3)	7790(6)	27(1)

Note. *U*(eq) is defined as one third of the trace of the orthogonalized U_{ij} tensor.

average K–O length changes from 3.06(22) at 213 K and from 3.09(21) at 274 K to 3.06(21) at 323 K for K(1) and from 2.95(14) and 2.94(13) to 2.95(10), respectively, for K(2) (where the numbers in parentheses indicate the standard deviation from the average value). These values are 2.40(6), 2.40(6), and 2.41(6) for the Na ion. According to the distortion theorem of Brown (24), K(1) is the main ion producing the transitions from paraelectric to ferreolectric and from this to paraelectric phase. This result is in agreement with the results of Melmed *et al.* (25), who studied the phase diagram of $Na[(NH_4)_xK_{1-x}]C_4H_4O_6 \cdot 4H_2O$, where the ferroelectricity of solid solution vanishes for $x > 0.1$. As the NH_4 ion is larger than the K ion, it must occupy the K(1) position, obstructing the transition. The role of K(1) can be also explained from the sum of bond valence in the K ion computed according to the Brown theory (26). The sum around K(1) is 0.76, 0.71, and 0.69 at 213, 274, and 323 K, respectively, while around K(2) it is equal to 0.93 at the three temperatures.

Hydrogen bond lengths at different temperatures are listed in Table 5. Every water molecule plays a different role in the crystal structure. All hydrogen bonds, with the exception of those from the O(8) water molecule, are between water molecules or between water and tartrate ions of the same chain along the *a*-axis.

Comparison between the structure at 274 K without electric dc field and the structure at 273 K with electric dc field (8). The possible formation of ferroelectric domains have no effect on our crystal structure refinement according to the obtained Flack coefficient. This can be corroborated if we compare the two structures, where it can be observed that the thermal anisotropic coefficients are greatest in the

TABLE 4
Bond Lengths (Å)

	213 K	274 K		323 K
		A	B	
K(1)–O(1)	2.8356(13)	2.818(3)	2.874(5)	2.842(3)
K(1)–O(9)(ii)	2.905(2)	2.958(7)	2.978(8)	2.995(7)
K(1)–O(8)(iii)	3.080(2)	3.118(6)	3.091(6)	3.119(7)
K(1)–O(10)(iv)	3.425(2)	3.405(6)	3.391(8)	3.400(8)
K(2)–O(7)(i)	2.797(2)	2.795(4)	2.813(5)	2.805(4)
K(2)–O(4)(iii)	2.8552(14)	2.862(6)	2.846(3)	2.851(3)
K(2)–O(5)	3.0002(14)	2.984(4)	3.014(4)	3.007(3)
K(2)–O(8)(i)	3.157(2)	3.118(6)	3.131(6)	3.135(7)
Na(1)–O(7)	2.344(2)	2.331(4)	2.346(4)	2.361(4)
Na(1)–O(10)(i)	2.347(2)			2.334(4)
Na(1)–O(10[a])(i)		2.334(4)	2.359(5)	
Na(1)–O(1)	2.3697(14)	2.370(3)	2.387(5)	2.381(4)
Na(1)–O(8)	2.365(2)	2.396(6)	2.353(5)	2.373(4)
Na(1)–O(3)(i)	2.465(2)			2.470(4)
Na(1)–O(3[a])(i)		2.475(6)	2.459(5)	
Na(1)–O(5)(i)	2.492(2)			2.512(4)
Na(1)–O(5[a])(i)		2.503(4)	2.499(5)	
O(1)–C(1)	1.272(2)	1.267(5)	1.272(7)	1.260(4)
O(2)–C(1)	1.251(2)	1.242(5)	1.262(6)	1.247(5)
O(3)–C(4)	1.262(2)	1.260(7)	1.266(6)	1.235(6)
O(4)–C(4)	1.260(2)	1.248(6)	1.248(5)	1.263(7)
O(5)–C(2)	1.431(2)	1.437(5)	1.415(7)	1.427(4)
O(6)–C(3)	1.423(2)	1.417(5)	1.416(5)	1.410(5)
C(1)–C(2)	1.541(2)	1.527(8)	1.530(5)	1.536(5)
C(2)–C(3)	1.533(2)	1.547(6)	1.528(6)	1.530(5)
C(3)–C(4)	1.541(2)	1.534(9)	1.521(5)	1.531(5)

Symmetry code:	at 213 and 323 K	at 274 K
	(i) = $-x+1/2$; $y-1/2$,$1-z$	$x+1/2$, $-y$, $1-z$
	(ii) = $x-1/2$, $1/2-y$, $1-z$	$x-1/2$, $1-y$, $1-z$
	(iii) = x, y, $z-1$	x, y, $z-1$
	(iv) = $x+1/2$, $-1/2-y$, $-z$	$x-1/2$, $1-y$, $-z$

[a] This atom belongs to the opposite molecule to that indicated in the column.

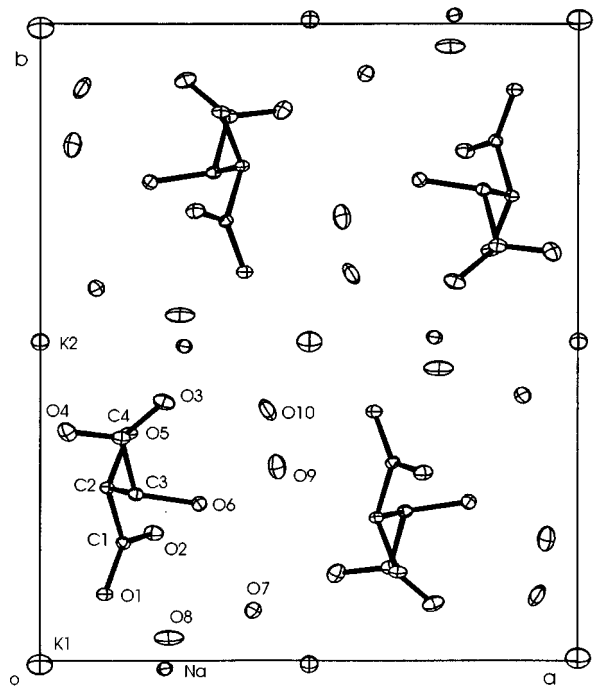

FIG. 2. Unit cell content viewed down the *c*-axis at 213 K, showing the label of atoms.

electric dc field structure. Another result that leads to the same result is the translational and librational tensor computed from our anisotropic thermal coefficients (Table 2) which does not shown an error due to the measured intensities by the quality of the crystal.

The second difference between the two structures is in the positions of the penta-coordinated water molecules O(8) and O(10). These atoms are those which show the largest displacement between the two structures [0.07 Å for O(8A); 0.05 Å for O(8B); 0.10 Å for O(10A) and 0.08 Å for (O10B)]. This fact suggests that these atoms must play an important role in the ferroelectric–paraelectric transition.

Comparison between the structures of paraelectric phases at 213 *and those at* 323 *K*. The main differences between the two paraelectric phases (high and low temperature) is in the systematic displacement along the *a*-axis of Na ion and the different orientation of the tartrate ion, which can be observed from the direction cosines of moments of inertia. The tartrate ion at high temperature is rotated 3° with rotation axis [012] with respect to the same ion at low temperature. This produces different displacement to water

TABLE 5
Hydrogen Bond Lengths (Å)

	213 K	274 K		323 K
		A	B	
O(1) ··· H(10A)–O(10)(i)	2.726(2)	2.719(6)	2.717(6)	2.738(6)
O(2) ··· H(5)–O(5)	2.610(2)	2.603(6)	2.574(6)	2.599(4)
O(2) ··· H(8A)–O(8)(ii)	2.764(2)	2.737(7)	2.721(7)	2.751(5)
O(3) ··· H(6)–O(6)	2.654(2)	2.642(6)	2.631(6)	2.642(5)
O(3) ··· H(8)–O(8[a])	2.706(2)	2.723(6)	2.694(6)	2.709(5)
O(4) ··· H(7)–O(7)(i)	2.870(2)	2.872(6)	2.885(6)	2.880(6)
O(6) ··· H(7)–O(7)	2.800(2)	2.799(6)	2.791(6)	2.806(5)
O(9) ··· H(10)–O(10)(i)	2.765(3)	2.761(9)	2.739(9)	2.777(9)
O(4) ··· H(9)–O(9[a])	2.813(2)	2.812(8)	2.813(8)	2.817(6)
O(10) ··· H(6)–O(6)	2.862(2)	2.825(7)	2.917(7)	2.912(6)
O(6) ··· H(9A)–O(9)	3.136(2)	3.148(6)	3.137(7)	3.151(7)

Symmetry code:
(i) = $x-1/2$, $1/2-y$, $1-z$
(ii) = x, y, $z-1$

[a] This atom belongs to the opposite molecule to that indicated in the column.

molecules, varying the bond lengths, especially those with the K(1) ion. The largest displacements are found for O(10) (0.083 Å), O(9) (0.091 Å), and O(8) (0.079 Å), which produce the lengthening of the K(1)–O(9) and K(1)–O(8) bond lengths and the shortening of the K(1)–O(10) bond length as the temperature is raised. Consequently, the K(1) potassium coordination polyhedron at high temperature is more regular than at low temperature. The variations in the bond lengths of K(2) coordination polyhedron are not significant. At low temperature, the intramolecular hydrogen bonded O of the acetato group shows the shortest C–O bond length. At high temperature, C(1)–O(2) and C(4)–O(3) bonds show the shortest C–O bond length while the O(10) $\cdots$ O(6) hydrogen bond length increases. From that, we conclude that there is a small but significant structural difference between the low- and high-temperature paraelectric phases, which were assumed to be identical in the structural model of Pepinsky (3, 12). On the other hand, the anisotropic thermal coefficients obtained for the two paraelectric phases and the translational and vibrational study (Table 2) do not justify the disorder assumed by the previous authors.

Comparison between the ferroelectric and paraelectric structures. The main difference among the ferroelectric structure and the two paraelectric structures (low- and high-temperature phases) is in the orientation of each tartrate ion with respect to crystallographic axes. The tartrate ion *A* of the ferroelectric phase is practically oriented in the same direction as the tartrate ion of the low-temperature paraelectric phase, while the tartrate ion *B* has the same orientation as the tartrate ion of the high-temperature paraelectric phase. (Notice about the director cosines of ion *B*. They have been computed on atomic positions related by a pseudo-twofold axis parallel to the *c*-axis with respect to atomic positions of paraelectric phases.) Consequent to the different orientation of tartrate ions, variations in the coordination and hydrogen bond lengths are observed. If we compare the position of water molecules between the ferroelectric phase and the low-temperature paraelectric phase the main displacements are 0.059 O(7A), 0.103 O(8A), 0.097 O(9A), 0.060 O(10A), 0.095 O(7B), 0.046 O(8B), 0.066 O(9B), and 0.122 O(10B). This fact produces variations in the interaction among the different ions and water molecules, which can be observed on the direction cosines of the librational tensor principal values, where the axes of the *B* ion are turned 45° with respect to the axes of ion *A*, and on the translational principal values, where ion *A* of the ferroelectric phase has the highest translational vibration along close to the *c*-axis, while the ion *B* has the highest translational vibration along the crystallographic plane *C*.

A structural and thermodynamic model for the double ferroelectric–paraelectric transition of Rochelle salt. If we analyze the variation of the sum of bond valence on K ions at different temperatures (K(1) = 0.76, 0.71, and 0.69 at 213, 274, and 323 K, respectively, and 0.93 for K(2) at the three temperatures), an important variation is not observed. As a consequence, this transition is not displacive. The hypothesis of Pepinsky (3, 12) on an order–disorder transition is not justified by the thermal parameters obtained in the two paraelectric phases and thermodynamically it is hard to assume an increase in the disorder when the temperature is lowered.

From the previous results we propose that the ferroelectric result is produced by two nonequivalent chains along the *a*-axis, each with a different polarization vector parallel to the *a*-axis. This hypothesis is similar to those proposed by Pepinsky (3, 12), but with two differences. The first is that we assume that a different displacement of water molecules and ions is responsible for this polarization, and not just for the variation of O(2)–C(1)–C(2)–O(5) torsion angle as indicated by Frazer *et al.* (3). The second is that Frazer *et al.* (3) assume that the two paralectric structures are similar, and the differences are only due to dilatation. The crystal structure of the high- and low-temperature paralectric phases show differences, which suggests different polarization vectors, so the high-temperature phase is produced by two chains, related by a twofold axis parallel to [001], each with a polarization vector P_{HT}, giving a result polarization vector zero. In the low-temperature paraelectric phase, analogously every chain has a polarization vector P_{LT}, but each two chains are related by the twofold axis parallel to [001]. The ferroelectric phase is an ordered solid solution of chains with polarization P_{HT} and others with polarization P_{LT}. The same model is used by us to explain the ferroelectric phase.

At constant pressure the Gibbs free energy variation ΔG accompanying the transformation paraelectric(LT)$\leftrightarrow$paraelectric(HT) is $\Delta G = \Delta H - T\Delta S$. The Gibbs free energy for the ferroelectric solid solution, using a regular model, is $G = G_{LT} + x\Delta H + wx(1-x) + RTx \ln x + RT(1-x) \ln(1-x) - RT \times \Delta S$, where x is the molar fraction of HT chains and $1-x$ of LT chains. The x values corresponding to the stable ferroelectric phase are defined by the condition $(\partial G/\partial x)_{T,p} = 0$, which leads to the implicit equation $\ln[(1-x)/x] = [\Delta H + w(1-2x)]/(RT) - \Delta S/R$. From the spontaneous polarization data measured by Hablützel (17) the value of x for each temperature has been determined, $|P_{HT} - P_{LT}| = 5 \times 10^{-7}$ C/cm^2, $\Delta H = 485$ cm^{-1}, $\Delta S = 1.76$ cm^{-1} K^{-1}, and $w = 152$ cm^{-1}. The deduced expression for the spontaneous polarization is similar to that used by Jona and Shirane (27) to explain from the Weiss-type theory the ferroelectricity of Rochelle salt. To corroborate our hypothesis the total polarization has been computed using the observed crystal structure coordinates at 274 K, using an ionic model and assuming $x = 0.5$ for this structure. The value obtained is 4.2×10^{-7}C/cm^2.

REFERENCES

1. G. Busch, *Condensed Matter News* **1,** 20–29 (1991).
2. A. C. Beevers and W. Hughes, *Proc. Roy. Soc. London A* **177,** 251–259 (1941).
3. B. C. Frazer, M. Mc Keown, and R. Pepinsky, *Phys. Rev.* **94,** 1435–1439 (1954).
4. F. Mazzi, F. Jona, and R. Pepinsky, *Zeift. Kristall.* **108,** 359–374 (1957).
5. S. Mitani, S. Fukui, I. Shibuya, Y. Shiozaki, K. Toyoda, and R. Pepinsky, *Ferroelectrics* **8,** 477–478 (1974).
6. Y. Iwata, N. Koyano and I. Shibuya, *Annu. Rep. Res. Reactor. Inst. Kyoto Univ.* **22,** 87–91 (1989).
7. Y. Iwata, S. Mitani, S. Fukui, and I. Shibuya (1989). *Annu. Rep. Res. Reactor. Inst. Kyoto Univ.* **22,** 14–26.
8. E. Suzuki, A. Amano, R. Nozaki, and Y. Shiozaki, *Ferroelectrics* **152,** 385–390 (1994).
9. T. Mitsui, *Phys. Rev.* **111,** 1259–1267 (1958).
10. B. Zeks, G. C. Shukla, and R. Blinc, *Phys. Rev. B* **3,** 2306–2309 (1971).
11. Y. Ishibashi and Y. Takagi, *J. Phys. Soc. Jpn.* **32,** 723–728 (1972).
12. R. Pepinsky, *in* "Physics of Electronic Ceramics," (L. Hench and D. Dove, Eds.), Chap. 7. Dekker, New York, (1972).
13. J. Laugier and A. Filhol, "Programme CELREF," 1978.
14. W. P. Mason, "Piezoelectric Cystals and Their Application to Ultrasonics." Van Nostrand, New York, 1950.
15. S. Mikaya, *J. Phys. Soc. Jpn.* **2,** 98 (1947).
16. M. A. Chernysheva, *Izvest. Akad. Nauk. S.S.S.R. Ser. Fiz.* **21,** 289–293 (1957).
17. J. Hablützel, *Helv. Phys. Acta* **12,** 489–497 (1939).
18. G. M. Sheldrick, *Acta Crystallogr. A* **46,** 467–472 (1990).
19. G. M. Sheldrick, "SHELXL, A Computer Program for Crystal Structure Determination." University of Göttingen, Germany, 1993.
20. H. D. Flack, *Acta Crystallogr. A* **39,** 867–881 (1983).
21. B. M. Craven, X. He and H. P. Weber, "Programme EKRT," University of Pittsburg, Pennsylvania, 1992.
22. W. Bronowska, *J. Appl. Cryst.* **14,** 203–207 (1981).
23. W. G. Cady, "Piezoelectricity." Mc Graw–Hill, New York, 1946.
24. I. D. Brown and D. Altermatt, *Acta Cryst. B* **41,** 244–247 (1985).
25. A. Melmed, F. Jona and R. Pepinsky, *Tech. Rep. N* 20, Wright Air Development Center, Contrac AF33(616)-2133. (1954). Unpublished.
26. I. D. Brown, *Acta Cryst. B* **48,** 553–572 (1992).
27. F. Jona and G. Shirane, *Ferroelectric crystals*, Dover pub., New York, pp 209–224 (1993).